Zhu *et al. Cancer Cell International* 2022, **22**(1):344
https://doi.org/10.1186/s12935-022-02764-y

Cancer Cell International

RESEARCH

Open Access

Transcriptome analysis of intestine from alk-SMase knockout mice reveals the effect of alk-SMase

Jiang Zhu[1†], Lingqi Wang[1,3†], Zhongwu Guo[4], Tao Zhang[1] and Ping Zhang[2*]

Abstract

Objective: Intestinal alkaline sphingomyelinase (alk-SMase) generates ceramide and inactivates platelet-activating factor associated with digestion and inhibition of cancer. There is few study to analyze the correlated function and characterize the genes related to alk-SMase comprehensively. We characterised transcriptome landscapes of intestine tissues from alk-SMase knockout (KO) mice aiming to identify novel associated genes and research targets.

Methods: We performed the high-resolution RNA sequencing of alk-SMase KO mice and compared them to wild type (WT) mice. Differentially expressed genes (DEGs) for the training group were screened. Functional enrichment analysis of the DEGs between KO mice and WT mice was implemented using the Database for Annotation, Visualization and Integrated Discovery (DAVID). An integrated protein–protein interaction (PPI) and Kyoto Encyclopedia of Genes and Genomes (KEGG) network was chose to study the relationship of differentially expressed gene. Moreover, quantitative real-time polymerase chain reaction (qPCR) was further used to validate the accuracy of RNA-seq technology.

Results: Our RNA-seq data found 97 differentially expressed mRNAs between the WT mice and alk-SMase gene NPP7 KO mice, in which 32 were significantly up-regulated and 65 were down-regulated, including protein coding genes, non-coding RNAs. Notably, the results of gene ontology functional enrichment analysis indicated that DEGs were functionally associated with the immune response, regulation of cell proliferation and development related terms. Additionally, an integrated network analysis was shown that some modules was significantly related to alk-SMase and with accordance of previously results. We chose 6 of these genes randomly were validated the accuracy of RNA-seq technology using qPCR and 2 genes showed difference significantly ($P < 0.05$).

Conclusions: We investigated the potential biological significant of alk-SMase with high resolution genome-wide transcriptome of alk-SMase knockout mice. The results revealed new insight into the functional modules related to alk-SMase was involved in the intestinal related diseases.

Keywords: Genome-wide, RNA-seq, Alk-SMase, Gene knockout

†Jiang Zhu and Lingqi Wang contributed equally to this work

*Correspondence: 035040@hrbmu.edu.cn

[2] International School of Public Health and One Health, Hainan Medical University, Haikou 571199, Hainan, China
Full list of author information is available at the end of the article

Background

Alk-SMase acts with phospholipase C to hydrolyse sphingomyelin (SM) to ceramide, inactivate platelet-activating factor (PAF) and reduce the formation of lysophosphatidic acid (LPA); these effects are all associated with the inhibition of colon cancer [1, 2]. Alk-SMase was discovered in 1969 [3], but the research history of intestinal alk-SMase has been less than 30 years in length. Alk-SMase is

expressed in the intestinal mucosa with low activity in the colon and high activity in the jejunum [4]. Alk-SMase, as a novel member of the nucleotide pyrophosphatase and phosphodiesterase (NPP) family, is also called ENPP7 [5]. The hydrolysis of exogenous SM was decreased in alk-SMase KO mice, suggesting an important role of this enzyme in SM hydrolysis in the gut [6].

Recently, some important biological effects of alk-SMase were reported [7]. Researchers purified the protein [8, 9], cloned the gene [5] and found essential roles for the enzyme in phospholipid hydrolysis [4, 10], anti-inflammation [11], anti-tumorigenesis [12], cell proliferation and cholesterol metabolism [13]. In addition, decreased alk-SMase activity was found in colon cancer and colitis [14–16]. Although the role of alk-SMase in the development of colon cancer has been studied, its physiological and pathological significance in the small intestine has not been well explored [3]. In previous studies [5, 6, 8, 9], we found that the functional difference between alk-SMase KO mice and wild-type (WT) mice was due to the deletion of an enzyme. However, the roles of related gene interactions and their transcriptome-level mechanisms have not been elucidated.

Genome-wide transcriptome analysis has become a promising tool to discover global changes in gene profiles under different conditions [17], but the molecular networks and gene interaction mechanisms in alk-SMase KO mice remain largely unknown. In this study, we detected a functional gene set correlated with alk-SMase by transcriptome analysis using a KO model. We performed the first high-resolution RNA sequencing of alk-SMase KO mice and compared them to WT mice. In addition, the transcriptional landscape of alk-SMase KO mice, which had unprecedented resolution, was used to study alk-SMase. Differentially expressed genes (DEGs) between the alk-SMase KO and WT groups were identified with the R package edgeR [18]. A functional enrichment analysis of the DEGs was conducted to understand the biological functions of alk-SMase and to further explore its related genes at the transcriptome level by constructing a gene-to-gene regulatory network that integrated Kyoto Encyclopedia of Genes and Genomes (KEGG) and Protein–Protein Interaction (PPI) data. We explored these biological relationships to further understand the metabolic characteristics and molecular regulation mechanisms of alk-SMase, and the results could provide a theoretical basis for further investigation of the phenotypes and other changes in alk-SMase KO mice.

Materials and methods

Animals and samples

The Alk-SMase KO mice were donated by Duan Rui-dong Group. The alk-SMase gene is located on chromosome 11 (Ensembl Gene ID:ENSMUSG 00000046697) in C57BL/6 mice. It was knocked out by the Cre-Loxp system as reported previously. The exon 2 was deleted by Cre recombinase to induce a shift of reading frame and it created an early stop codon and resulted in blocking the translation of the protein. The genotype and phenotype of all mice were assayed by PCR and fecal alk-SMase activity. All mice were housed in the animal facilities at Daqing campus, Harbin Medical University, which were fed commercial standard pellets with free access to water. The mice were anaesthetized by inhaled isoflurane and euthanized by cervical dislocation. All experimental protocols were approved by the Animal Ethics Committee of Harbin Medical University, China. All mice were killed by cervical dislocation under inhaled isoflurane anesthesia and we obtained three matched pairs of intestinal tissue from 3 WT mice and 3 KO mice, respectively. In functional studies, we used alk-SMase knockout mice for experiments. In the DSS-induced colonic inflammatory tumor model, inflammation in alk-SMase KO mice was significantly more intense than in wild type (WT) mice, while in colon cancer models, the number of tumors in KO mice. The degree of malignancy and tumors are also much higher than in WT mice. Our research group have found the important function of alk-SMase in gut, such as anti-inflammatory effect, anti-tumorigenesis, phospholipids hydrolysis and cholesterol metabolism.

RNA extraction, sequencing and data processing

Total RNA from the middle small intestinal mucosa of every mouse was extracted with the TRIzol method according to the manufacturer's instructions. The RNA samples were deeply sequenced using the Illumina HiSeq 2500 platform after further clean-up using Qiagen RNeasy Mini columns, and 50 bp single-end reads were generated [19, 20]. Quality control was performed by FastQC (http://www.bioinformatics.babraham.ac.uk/projects/fastqc/), and trim-galore was used to remove the adapter sequences and obtain clean reads. The subsequent processes, including mapping to the reference genome, assembling and gene expression analysis, were carried out by the HISAT2 and StringTie pipeline [21]. HISAT2 was chosen to map the reads to the mouse reference genome (mm10) from the UCSC Genome Browser database, resulting in an alignment rate of 94.18–95.36%.

Identification of DEGs

The R package edgeR was used to identify DEGs in the intestinal tissue of the knockout group and control group based on fold change > 1.5 (or < 2/3) and FDR < 0.05. The fold change value refers to the multiplier of the gene expression in the treatment group relative to the control group. The fragments per kilobase per million

reads (FPKM) values and fold changes of all genes were extracted from the RNA-seq results for further analyses. Three WT samples and three KO samples were compared to find significantly up- and down regulated genes. The heatmaps of the most significantly up regulated and down regulated transcripts were generated with the R command heatmap.2.

Gene Ontology and KEGG pathway enrichment analyses

In this work, functional enrichment analysis of the DEGs between KO mice and WT mice was implemented using the Database for Annotation, Visualization and Integrated Discovery (DAVID; http://david.abcc.ncifcrf.gov) [22]. Gene Ontology (GO) categories in the biological process ontology and KEGG pathways were identified with a significant threshold p-value ≤ 0.05 and FDR ≤ 0.01.

Construction of the gene regulatory network and identification of significant genes

In light of the complexity of gene regulation, we expected to find interactions between ENPP7 and DEGs. The protein–protein interaction data were obtained from two PPI databases, Biological General Repository for Interaction Datasets (BioGRID) [23] and Reactome [24]. To obtain more comprehensive interaction information, we used the union data of these two databases as background. In addition, a KEGG network was established based on relationships between genes in the pathway using in-house Perl programs. Eventually, a gene regulatory network was constructed by merging the PPI and KEGG networks. The 97 DEGs were set as seed genes and then mapped into the integrated background network to extract the PPI and KEGG sub-network. The sub-network was composed of these seed genes and the nearby genes (within a one-step distance from the seed genes) in an integrated background network. The network was constructed using Cytoscape 3.3.0 [25], an open-source program used to establish biological networks.

RT-PCR verification

The mRNA levels of all genes were quantified by real-time PCR. The cDNA was generated using a ReverTra Ace qPCR RT Master Mix kit (Toyobo, China). All primers were obtained from Invitrogen and designed using reference sequences published by the National Center for Biotechnology Information. qPCR was performed on a Roche Light Cycler 480. The reaction volume was 20 µl, including 10 µl of SYBR Green Realtime PCR Master Mix kit (Toyobo, China), 2 µl of diluted cDNA template, and 0.8 µl of 10 µM primers to activate the polymerase, followed by 40 cycles of 95 °C for 15 s and 65 °C for 30 s. The melting curve analysis was performed to confirm that a single product was amplified, and the cycle threshold (CT) was determined by Roche System Software. The relative expression of each mRNA was normalized to the level of the housekeeping gene GAPDH using the $2^{-\Delta\Delta CT}$ method. Six DEGs were chosen for the experiment. The t-test was used for significance testing between the WT and KO groups, and a p-value ≤ 0.05 was considered significant.

Results

Analysis of transcriptome characteristics

Whole transcriptome sequencing was conducted on three matched samples of alk-SMase KO mice and WT mice. In total, approximately 113 million single-end reads were generated by HiSeq 2500 ultra-high-throughput sequencing systems, with an average of 18.9 million reads per sample. After trimming the raw data, the clean data were successfully mapped to the reference genome, and all probable transcripts in the genome were assembled using StringTie. Table 1 lists the read mapping rates for all six samples, which were more than 90%. Quality control of the fastq data produced by the high-throughput sequencers was performed by FastQC software. The expression of all transcripts was normalized by edgeR, and the results were in agreement with a high correlation (Fig. 2D). Although the mRNA expression patterns between the two groups of samples were very similar, numerous differences were observed. The Perl program Circos v0.62 was used to plot genome-wide expression profiles from the intestinal tissue samples from KO mice and WT mice; the data are shown as a circular map in Fig. 1 and a probability density graph in Fig. 2A. Transcripts with low expression (FPKM < 1) in more than 4 samples were removed from the subsequent analysis.

Identification of DEGs in KO mice

We performed bioinformatics analyses to investigate the DEGs and functional pathways that characterized the DEGs in our transcriptome. The R package edgeR was used to identify the DEGs. A total of 97 mRNAs were differentially expressed in the intestinal tissue of

Table 1 The overall read mapping rate

Sample	Mapping rate (%)	Input reads	Mapped reads
K79S	95.11	15922606	15143940
K82S	94.85	21424125	20319836
K86S	94.38	12969342	12239110
W83S	95.36	22015543	20994022
W89S	94.18	21904848	20629985
W90S	94.91	16723969	15872812

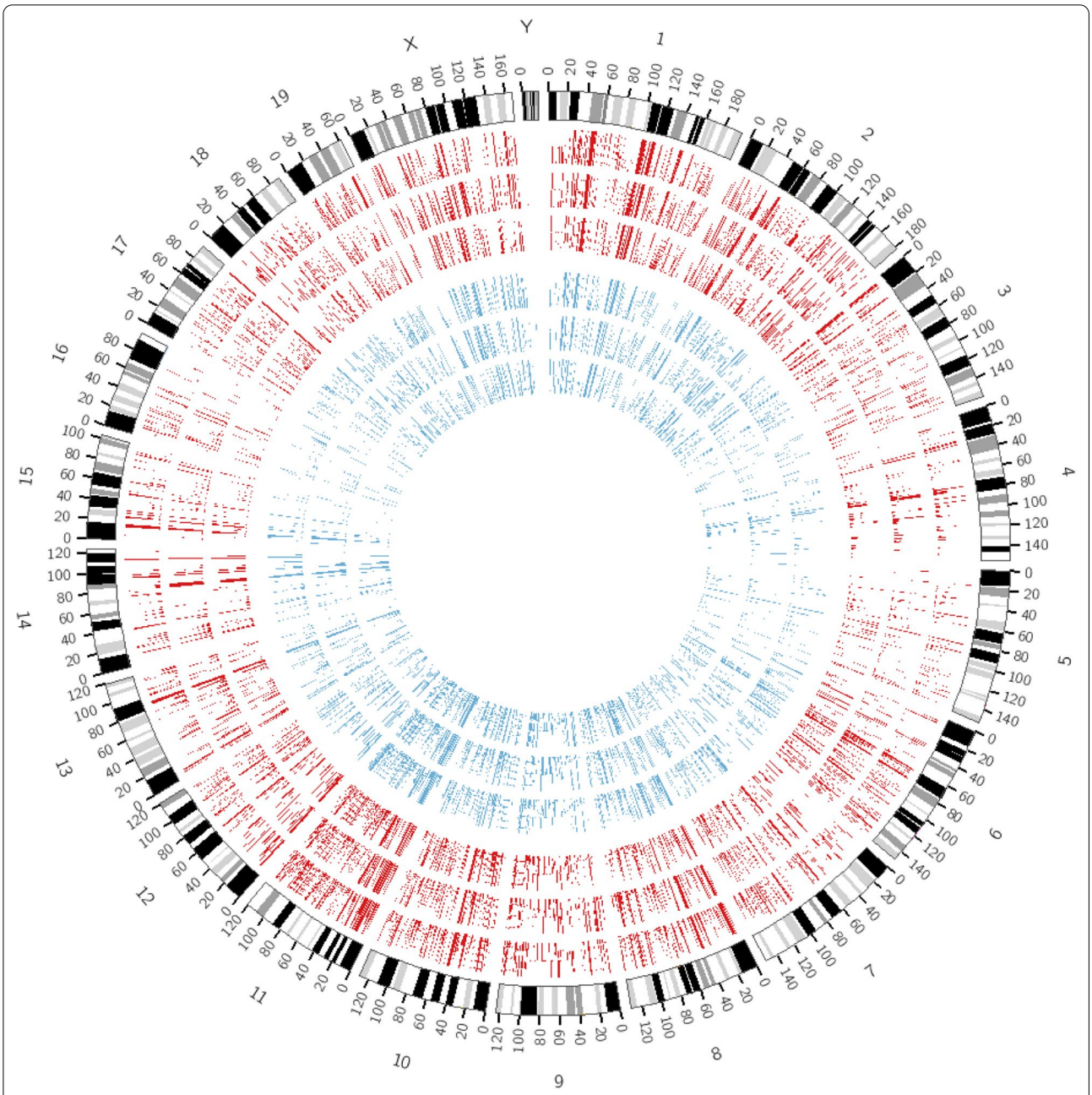

Fig. 1 Circos plot of mRNA expression data. Circos v0.62 software was used to visualise global tissue mRNA expression in WT mice and KO mice. Data are shown as a circular map. The three KO samples are shown in the outer three rings, and the inner three rings represent the WT samples. The blue bars represent WT mice, and the red bars represent KO mice

KO mice compared with that of WT mice, including 32 significantly up regulated and 65 down regulated mRNAs (see Additional file 1). Hierarchical clustering analysis showed that the samples from the KO mice collapsed into one cluster, and those from the WT mice collapsed into the other cluster, suggesting that the expression levels of these DEGs in the KO mice were significantly different from those in the WT mice (Fig. 2C). In Fig. 2B, a heterologous gene expression volcano plot [26] also displays the DEG results. Red dots indicate genes with no statistically significant differences in gene expression, and cyan dots in the figure represent DEGs with statistical significance.

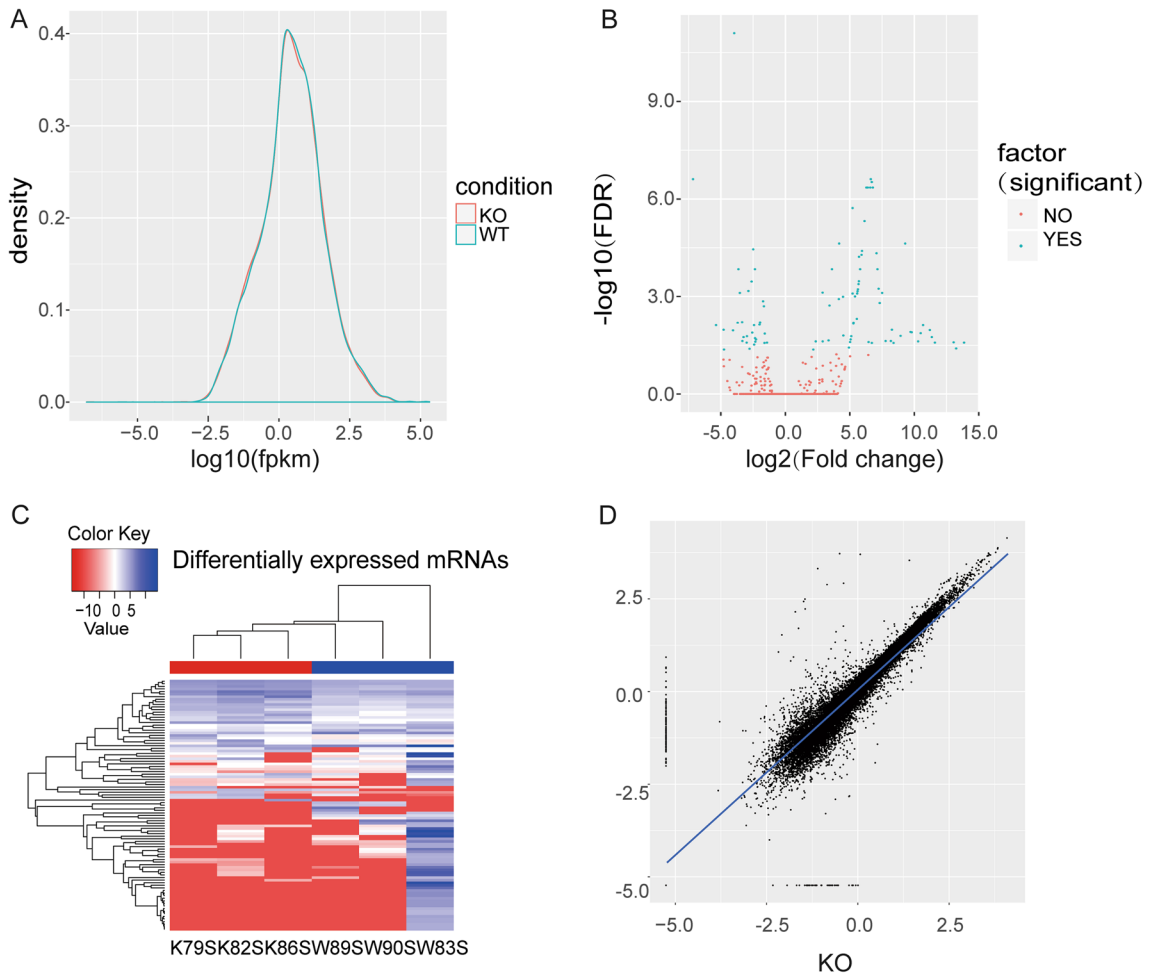

Fig. 2 Hierarchical clustering and transcriptome characteristics. **A** Transcript expression distribution density graph of different samples. **B** Volcano plots of the distribution of gene expression. Red dots indicate genes with no statistically significant differences in gene expression, and cyan dots in the figure represent DEGs with statistical significance. **C** Two-way hierarchical clustering of DEGs in KO samples and WT samples. **D** Correlation graph of two types of different samples

To explore the potential biological functions of the DEGs, a functional enrichment analysis was performed for the DEGs using the DAVID functional annotation tool. With a p-value ≤ 0.05 as the threshold, the results indicated that the DEGs were mainly involved in metabolic-process-associated pathways and biological processes including carbohydrate catabolic process, amylase activity, fatty acid binding, and positive regulation of immune response (Fig. 3B–D). These DEGs were enriched in ten pathways, including asthma, gastric acid secretion, starch and sucrose metabolism, fat digestion and absorption, carbohydrate digestion and absorption, glycerolipid metabolism, and metabolic pathways (Fig. 3A).

Identification of significant genes by EMODE in an integrated PPI and KEGG network

As a result of the complexity of gene regulation, we expected to find interaction and regulation among the DEGs in *ENPP7* KO mice. In this study, we selected an integrated PPI and KEGG pathway-based biological network as a background network, in which a total of two sets of mouse PPI data were obtained from BioGRID and Reactome, and the pathways containing DEGs were considered enriched. We mapped 97 seed DEGs into the integrated background network to extract the sub-network. The sub-network was composed of these seed genes and the neighboring genes in the integrated background network (within one step of the seed genes) (Fig. 4).

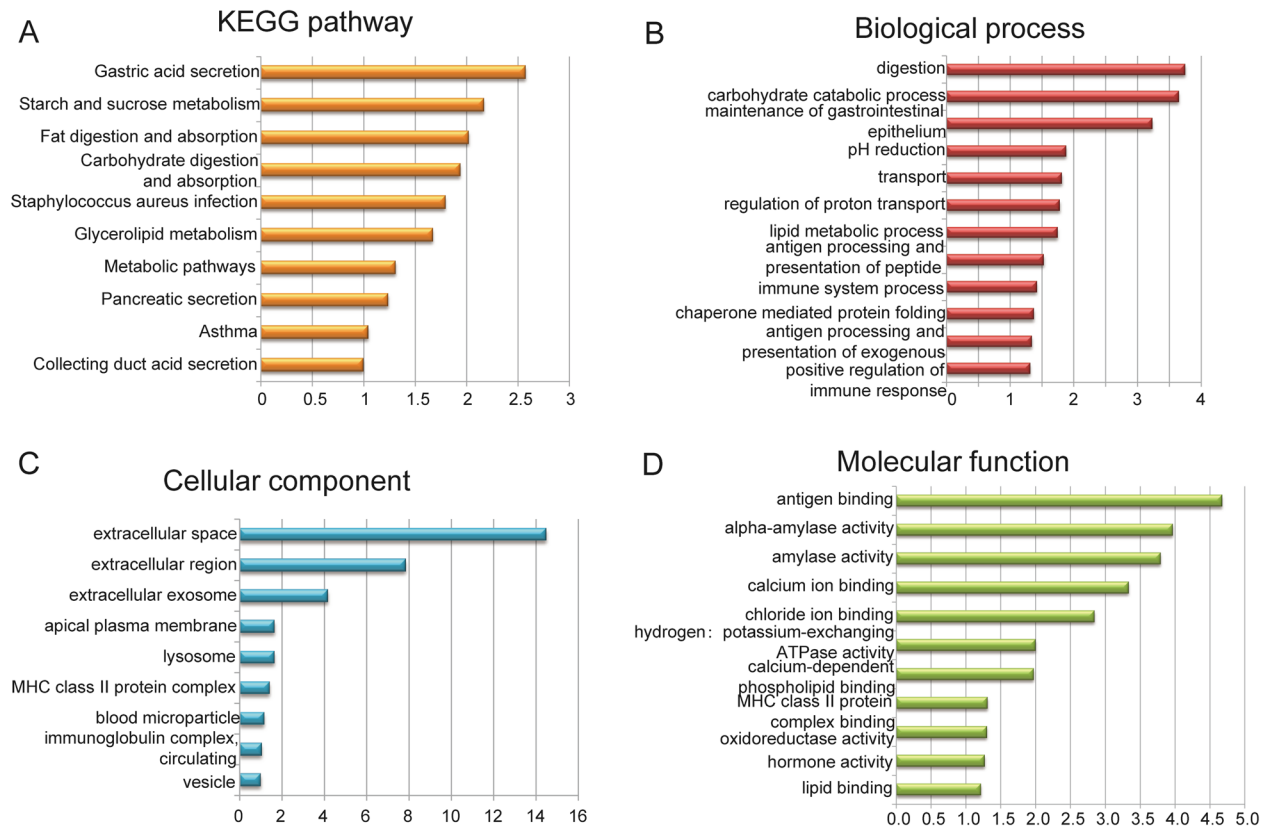

Fig. 3 Functional enrichment analysis and enrichment map for DEGs. GO and KEGG enrichment analyses were performed using DAVID with $p < 0.05$. The results revealed the GO functions and KEGG pathways associated with DEGs. **A** KEGG pathway analysis of DEGs using DAVID. **B** Biological process terms of DEGs using DAVID. **C** Cellular component terms of DEGs using DAVID. **D** Molecular function terms of DEGs using DAVID

Considering the genes connected in the network and genes in the same pathway that were thought to have similar and biologically related functions, dividing these highly connected genes into groups by network analysis may be useful for potential functional processes in a manner complementary to standard differential expression analysis. In the sub-network, a small number of nodes had high degrees, while many had low degrees. The hub genes in this sub-network included *Cyp3a44, Pnliprp1, Mogat1, Pla2g1b, Amy2a4, Amy2a3, Amy2a5, Akr1b8, Aldh3a1* and *Ldhb* (Table 2).

Validation of DEGs by real-time PCR

To validate the accuracy of the RNA-seq data, we further analyzed the expression of six randomly selected transcripts by RT-PCR. As shown in Fig. 5, the results of the RT-PCR experiment suggested that the expression of all 6 transcripts was consistent with the RNA-seq data, and the *H2-AB1* and *SPP1* genes showed significant differences by t-test ($P < 0.05$) [27], the additional file shows this in more detail (see Additional file 2). However, the differential expression analysis included three biological replicates, and a subset of the transcripts showed opposite expression patterns between replicates, indicating individual differences. In addition, although the mean expression values in the figures showed a noticeable difference, it was not statistically significant.

Discussion

Some biological effects of alk-SMase have been reported, including the essential roles ofthis enzyme, including anti-inflammatory and anti-tumorigenesis effects, phospholipid hydrolysis and cholesterol absorption [28]. However, the mechanism of action of alk-SMase in the intestine remains poorly understood. Here, we performed a comprehensive analysis to investigate the interactions and relationship between alk-SMase (*ENPP7*) and other genes. The objective to find out the key genes of alk-SMase interactions in the intestine. Notably, decreased alk-SMase activity has been reported in colon cancer and colitis [29]. Although the role of alk-SMase in the development of colon cancer has been studied, the biological significance and interactions of this enzyme have not been well studied in the intestine. Transcriptome analysis

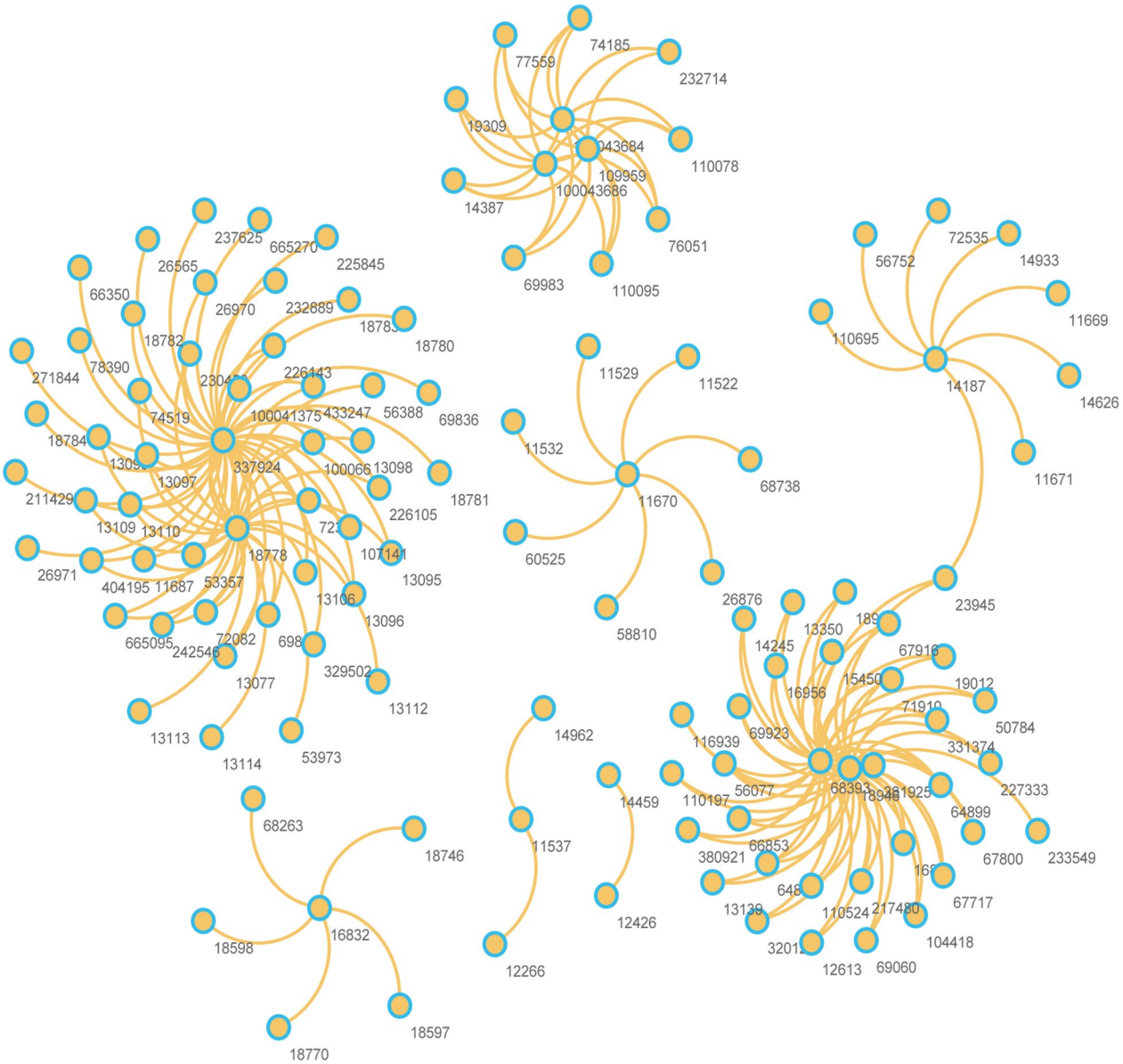

Fig. 4 The network was constructed by mapping the DEGs to a PPI and KEGG integrated network. The sub-network was extracted from the PPI-KEGG integrated network by one-step neighbour nodes

is an effective way to study and understanding the basis of phenotypic variation in different conditions [30]. Here, we used transcriptome profile analysis to reveal DEGs. A total of 97 DEGs were identified, and these genes were related to immune-related diseases and lipid metabolism and carbohydrate catabolic processes. It has been found that some pathway and GO terms are closely related to lipid and glucose metabolism and cell differentiation [31, 32], and proliferation [33]. We expected that the knock-out model of alk-SMase gene could be used to analyze the interactions between alk-Smash and other genes, or the regulation of related genes, so as to play a protective role in the intestinal mucosal barrier, as we have found in the experiments, or other biological functions. The absence of NPP7 caused alterations in gene expression in the intestine transcriptomes in KO mice. The alteration of intestinal function is caused by the loss of expression of intestinal basic sphingomyelin, which affects bile acid metabolism, bile acid intestinal hepatic circulation and the expression of other related genes. Among the DEGs, a large number of genes are worthy of subsequent analyses, and transcriptome sequencing is a very effective

Table 2 Hub genes in the PPI and KEGG network

Gene	Regulation	Degree
Cyp3a44	Up	44
Pnliprp1	Up	34
Mogat1	Down	33
Pla2g1b	Down	31
Amy2a4	Down	9
Amy2a3	Up	9
Amy2a5	Down	9
Akr1b8	Up	8
Aldh3a1	Up	7
Ldhb	Up	7

method to select functional gene sets for related pathways. For example, *Muc1* is highly expressed in colon cancer and has been reported as a new target antigen for tumour vaccines. In addition, serum *Muc1* is a new indicator that may be involved in tumour invasion, which can assist in the early diagnosis of colon cancer [34]. Meanwhile, Annexin A13 (*ANXA13*) is a surface protein of *Lactobacillus reuteri* [35]. Mucosal adhesion proteins are bound to the surfaces of the intestinal epithelial cells by *ANXA13* and *PALM*. *ANXA13* is a receptor-like molecule and an immunoregulatory factor with anti-inflammatory effects [36]. Together, the DEGs that we identified maintain the intestinal mucosal barrier function of alk-SMase in the intestine.

Numerous transcription changes involving complex gene pathways, including metabolism, immune response and inflammation, have been described. RNA sequencing allows rapid quantification of gene expression in small number of tissue, whether in whole or in a targeted way. In order to verify the potential biological relationships between DEGs, we constructed a network based on PPI and pathway information. By arranging the first ten degrees, ten central genes were identified from the subnet. Up regulation of *Mogat1* conceivably mediates hepatic steatosis and insulin resistance through increasing intracellular diacylglycerol content [37], consistent with our results. PLA2G1B mediates lipid absorption, and PLA2G1B-derived metabolic products contribute to cardiometabolic diseases, including obesity, hyperinsulinaemia, and atherosclerosis [38]. In the future, we can further analyze the functions of these genes.

To examine the accuracy of the RNA-seq data, we analyzed the expression of six transcripts by quantitative real-time PCR. RT-PCR results showed that all 6 transcription levels were consistent with RNA-seq results, and there were significant differences between H 2-AB 1 and SPP 1 genes through T-test. We investigated H2-AB1 in the literature and found that H2-AB1 was differentially expressed in endothelial cell RNA isolated from control and hyperlipidaemic prelesion mice by expression array analysis [39]. The level of H2-AB1 was highly increased in allergic rhinitis, and it was associated with the pathogenesis of allergic rhinitis [40]. Another differentially expressed transcript, secreted

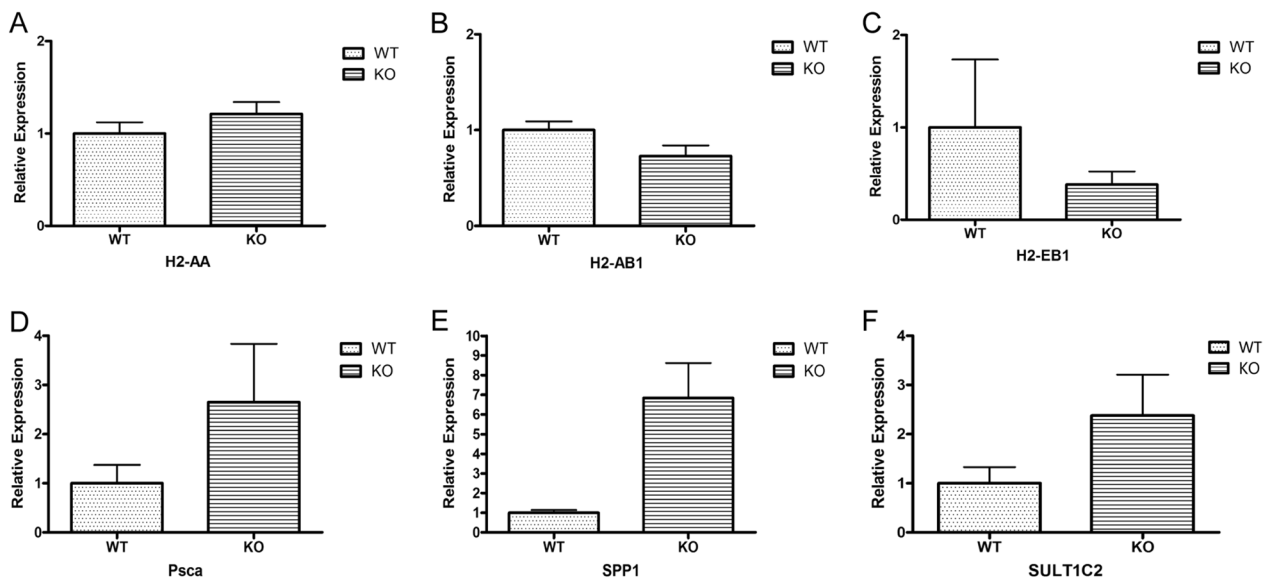

Fig. 5 Results of RT-PCR performed on RNA extracted from WT mice and ENPP7 KO mice. **A**–**F** Represent H2-AA, H2-AB1, H2-EB1, Psca, SPP1, and SULT1C2, respectively

phosphoprotein 1 (SPP1), a highly phosphorylated protein, plays important roles in physiological processes such as inflammatory responses, calcification, organ development, carcinogenesis response and immune cell function [41, 42], suggesting that SPP1 is also an important marker in the alk-SMase KO model and may participate in functional and phenotypic effects.

A comprehensive analysis of the experiment showed some exciting results. A large number of immunoglobulin-related genes, which have been found to affect immune function in the mucosal barrier, were among the DEGs. Insulin growth factor binding protein was also a gene of interest. Whether this enzyme is related to insulin metabolism or diabetes merits further experiments. A large number of lipid-metabolism-related enzymes are associated with alk-SMase, and tight junction proteins provide important antibodies for our analysis of mucosal barrier function. Overall, the RNA-seq analysis provided valuable guidance for future experiments.

Conclusions

In this study, DEGs was successfully identified and characterized in the alk-SMase gene KO model of mice. A total of 97 DEGs, including Mogat1, Pla2g1b, and Amy2a4, were identified across the whole genome. Our results showed that these DEGs were enriched in metabolism-related pathways. Our study provides the first systematic genome-wide analysis of the alk-SMase knockout model, alk-SMase plays an important role in the in intestinal sphingomyelin hydrolysis. The expression levels of SPP1 and H2-AB1 were effected in intestine tissues lacking alk-SMase expression.

Abbreviations

alk-SMase: Alkaline sphingomyelinase; BioGRID: Biological general repository for interaction datasets; DAVID: Database for annotation visualization and integrated discovery; GO: Gene Ontology; KEGG: Kyoto encyclopedia of genes and genomes; KO: Knoc kout; qPCR: Quantitative real-time polymerase chain reaction; WT: Wild type.

Supplementary Information

The online version contains supplementary material available at https://doi.org/10.1186/s12935-022-02764-y.

Additional file 1. The list of differentially expressed genes

Additional file 2. The original experimental data of qPCR

Acknowledgements

We thank Kylee P, Ph.D., from Wiley Editing services (https://wileyeditingservices.com/en/), for editing the English text of a draft of this manuscript.

Author contributions

JZ the first author, charging for design, data aggregation and writing; LQW data collecting and discussing with the first author; ZWG participating in design and administrative services; TZ assisting in statistical analysis; PZ the correspondence author, providing funding and direction for the project. All authors read and approved the final manuscript.

Funding

This work was supported by grants from Scientific Research Fund of Harbin Medical University-Daqing [Grant Number 2018XN-15]; Wu liande Youth Training Fund of Harbin Medical University [JFWLD202001] and Scientific Research Project of Heilongjiang Provincial Health Commission [Grant Number 2019-075].

Availability of data and materials

All data generated or analysed during this study have been submitted to the Genome Expression Omnibus (GEO) database, the accession number is GSE114608 (https://www.ncbi.nlm.nih.gov/geo/query/acc.cgi?acc=GSE114608). To review GEO accession GSE114608: Go to https://www.ncbi.nlm.nih.gov/geo/query/acc.cgi?acc=GSE114608. Enter token qtezmuculhihfgn into the box.

Declarations

Ethics approval and consent to participate

The animal studies were approved by the Animal Ethical and Welfare Committee of Harbin Medical University, Daqing Campus (approval number HMUDQ-2015-068), and this study was carried out in accordance with the guidelines and regulations established by this committee.

Consent for publication

Not applicable.

Competing interests

The authors declare no potential conflicts of interest.

Author details

[1]Medical Laboratory Technology College, Daqing Campus of Harbin Medical University, Daqing 163319, Heilongjiang, China. [2]International School of Public Health and One Health, Hainan Medical University, Haikou 571199, Hainan, China. [3]Department of Laboratory Diagnosis, The fifth Affiliated Hospital of Harbin Medical University, Daqing 163319, Heilongjiang, China. [4]General Surgery, Daqing Oil General Hospital, Daqing 163319, Heilongjiang, China.

Received: 29 January 2022 Accepted: 11 October 2022
Published: 9 November 2022

References

1. Zhang P, Chen Y, Cheng Y, Hertervig E, Ohlsson L, Nilsson A, Duan RD. Alkaline sphingomyelinase (NPP7) promotes cholesterol absorption by affecting sphingomyelin levels in the gut: a study with NPP7 knockout mice. Am J Physiol Gastrointest Liver Physiol. 2014;306:G903–8.
2. Wu J, Liu F, Nilsson A, Duan RD. Pancreatic trypsin cleaves intestinal alkaline sphingomyelinase from mucosa and enhances the sphingomyelinase activity. Am J Physiol Gastrointest Liver Physiol. 2004;287:G967–73.
3. Nilsson A. The presence of spingomyelin- and ceramide-cleaving enzymes in the small intestinal tract. Biochim Biophys Acta. 1969;176:339–47.
4. Nilsson A, Duan RD. Alkaline sphingomyelinases and ceramidases of the gastrointestinal tract. Chem Phys Lipids. 1999;102:97–105.
5. Duan RD, Bergman T, Xu N, Wu J, Cheng Y, Duan J, Nelander S, Palmberg C, Nilsson A. Identification of human intestinal alkaline sphingomyelinase as a novel ecto-enzyme related to the nucleotide phosphodiesterase family. J Biol Chem. 2003;278:38528–36.
6. Zhang Y, Cheng Y, Hansen GH, Niels-Christiansen LL, Koentgen F, Ohlsson L, Nilsson A, Duan RD. Crucial role of alkaline sphingomyelinase in sphingomyelin digestion: a study on enzyme knockout mice. J Lipid Res. 2011;52:771–81.
7. Nilsson A, Duan RD, Ohlsson L. Digestion and absorption of milk phospholipids in newborns and adults. Front Nutr. 2021;8: 724006.

8. Cheng Y, Nilsson A, Tomquist E, Duan RD. Purification, characterization, and expression of rat intestinal alkaline sphingomyelinase. J Lipid Res. 2002;43:316–24.
9. Duan RD, Cheng Y, Hansen G, Hertervig E, Liu JJ, Syk I, Sjostrom H, Nilsson A. Purification, localization, and expression of human intestinal alkaline sphingomyelinase. J Lipid Res. 2003;44:1241–50.
10. Wu J, Cheng Y, Palmberg C, Bergman T, Nilsson A, Duan RD. Cloning of alkaline sphingomyelinase from rat intestinal mucosa and adjusting of the hypothetical protein XP_221184 in GenBank. Biochim Biophys Acta. 2005;1687:94–102.
11. Andersson D, Kotarsky K, Wu J, Agace W, Duan RD. Expression of alkaline sphingomyelinase in yeast cells and anti-inflammatory effects of the expressed enzyme in a rat colitis model. Dig Dis Sci. 2009;54:1440–8.
12. Hertervig E, Nilsson A, Cheng Y, Duan RD. Purified intestinal alkaline sphingomyelinase inhibits proliferation without inducing apoptosis in HT-29 colon carcinoma cells. J Cancer Res Clin Oncol. 2003;129:577–82.
13. Feng D, Ohlsson L, Ling W, Nilsson A, Duan RD. Generating ceramide from sphingomyelin by alkaline sphingomyelinase in the gut enhances sphingomyelin-induced inhibition of cholesterol uptake in Caco-2 cells. Dig Dis Sci. 2010;55:3377–83.
14. Hertervig E, Nilsson A, Bjork J, Hultkrantz R, Duan RD. Familial adenomatous polyposis is associated with a marked decrease in alkaline sphingomyelinase activity: a key factor to the unrestrained cell proliferation? Br J Cancer. 1999;81:232–6.
15. Hertervig E, Nilsson A, Nyberg L, Duan RD. Alkaline sphingomyelinase activity is decreased in human colorectal carcinoma. Cancer. 1997;79:448–53.
16. Sjoqvist U, Hertervig E, Nilsson A, Duan RD, Ost A, Tribukait B, Lofberg R. Chronic colitis is associated with a reduction of mucosal alkaline sphingomyelinase activity. Inflamm Bowel Dis. 2002;8:258–63.
17. Ferreira PG, Jares P, Rico D, Gomez-Lopez G, Martinez-Trillos A, Villamor N, Ecker S, Gonzalez-Perez A, Knowles DG, Monlong J, Johnson R, Quesada V, Djebali S, Papasaikas P, Lopez-Guerra M, Colomer D, Royo C, Cazorla M, Pinyol M, Clot G, Aymerich M, Rozman M, Kulis M, Tamborero D, Gouin A, Blanc J, Gut M, Gut I, Puente XS, Pisano DG, Martin-Subero JI, Lopez-Bigas N, Lopez-Guillermo A, Valencia A, Lopez-Otin C, Campo E, Guigo R. Transcriptome characterization by RNA sequencing identifies a major molecular and clinical subdivision in chronic lymphocytic leukemia. Genome Res. 2014;24:212–26.
18. Robinson MD, McCarthy DJ, Smyth GK. edgeR: a Bioconductor package for differential expression analysis of digital gene expression data. Bioinformatics. 2010;26:139–40.
19. Alves MG, Perez-Sayans M, Padin-Iruegas ME, Reboiras-Lopez MD, Suarez-Penaranda JM, Lopez-Lopez R, Carta CF, Issa JS, Garcia-Garcia A, Almeida JD. Comparison of RNA extraction methods for molecular analysis of oral cytology. Acta Stomatol Croat. 2016;50:108–15.
20. Li D, Ren W, Wang X, Wang F, Gao Y, Ning Q, Han Y, Song T, Lu S. A modified method using TRIzol reagent and liquid nitrogen produces high-quality RNA from rat pancreas. Appl Biochem Biotechnol. 2009;158:253–61.
21. Pertea M, Kim D, Pertea GM, Leek JT, Salzberg SL. Transcript-level expression analysis of RNA-seq experiments with HISAT, StringTie and Ballgown. Nat Protoc. 2016;11:1650–67.
22. da Huang W, Sherman BT, Lempicki RA. Systematic and integrative analysis of large gene lists using DAVID bioinformatics resources. Nat Protoc. 2009;4:44–57.
23. Breitkreutz BJ, Stark C, Reguly T, Boucher L, Breitkreutz A, Livstone M, Oughtred R, Lackner DH, Bahler J, Wood V, Dolinski K, Tyers M. The BioGRID interaction database: 2008 update. Nucleic Acids Res. 2008;36:D637–40.
24. Vastrik I, D'Eustachio P, Schmidt E, Gopinath G, Croft D, de Bono B, Gillespie M, Jassal B, Lewis S, Matthews L, Wu G, Birney E, Stein L. Reactome: a knowledge base of biologic pathways and processes. Genome Biol. 2007;8:R39.
25. Shannon P, Markiel A, Ozier O, Baliga NS, Wang JT, Ramage D, Amin N, Schwikowski B, Ideker T. Cytoscape: a software environment for integrated models of biomolecular interaction networks. Genome Res. 2003;13:2498–504.
26. Costentin C, Saveant JM. Heterogeneous molecular catalysis of electrochemical reactions: volcano plots and catalytic Tafel plots. ACS Appl Mater Interfaces. 2017;9:19894–9.
27. Livak KJ, Schmittgen TD. Analysis of relative gene expression data using real-time quantitative PCR and the 2(-Delta Delta C(T)) Method. Methods. 2001;25:402–8.
28. Piccolo BD, Graham JL, Kang P, Randolph CE, Shankar K, Yeruva L, Fox R, Robeson MS, Moody B, LeRoith T, Stanhope KL, Adams SH, Havel PJ. Progression of diabetes is associated with changes in the ileal transcriptome and ileal-colon morphology in the UC Davis Type 2 Diabetes Mellitus rat. Physiol Rep. 2021;9: e15102.
29. Gorelik A, Liu F, Illes K, Nagar B. Crystal structure of the human alkaline sphingomyelinase provides insights into substrate recognition. J Biol Chem. 2017;292:7087–94.
30. Zhang S, Wang Y, Chen M, Sun L, Han J, Elena VK, Qiao H. CXCL12 methylation-mediated epigenetic regulation of gene expression in papillary thyroid carcinoma. Sci Rep. 2017;7:44033.
31. Ding L, Liang XG, Zhu DY, Lou YJ. Icariin promotes expression of PGC-1alpha, PPARalpha, and NRF-1 during cardiomyocyte differentiation of murine embryonic stem cells in vitro. Acta Pharmacol Sin. 2007;28:1541–9.
32. Ding L, Liang XG, Lou YJ. Time-dependence of cardiomyocyte differentiation disturbed by peroxisome proliferator-activated receptor alpha inhibitor GW6471 in murine embryonic stem cells in vitro. Acta Pharmacol Sin. 2007;28:634–42.
33. Zhong X, Xiu LL, Wei GH, Liu YY, Su L, Cao XP, Li YB, Xiao HP. Bezafibrate enhances proliferation and differentiation of osteoblastic MC3T3-E1 cells via AMPK and eNOS activation. Acta Pharmacol Sin. 2011;32:591–600.
34. Yu XT, Xu YF, Huang YF, Qu C, Xu LQ, Su ZR, Zeng HF, Zheng L, Yi TG, Li HL, Chen JP, Zhang XJ. Berberrubine attenuates mucosal lesions and inflammation in dextran sodium sulfate-induced colitis in mice. PLoS ONE. 2018;13: e0194069.
35. Matsuo Y, Miyoshi Y, Okada S, Satoh E. Receptor-like Molecules on Human Intestinal Epithelial Cells Interact with an Adhesion Factor from Lactobacillus reuteri. Biosci Microbiota Food Health. 2012;31:93–102.
36. Jiang G, Wang P, Wang W, Li W, Dai L, Chen K. Annexin A13 promotes tumor cell invasion in vitro and is associated with metastasis in human colorectal cancer. Oncotarget. 2017;8:21663–73.
37. Ramon-Krauel M, Pentinat T, Bloks VW, Cebria J, Ribo S, Perez-Wienese R, Vila M, Palacios-Marin I, Fernandez-Perez A, Vallejo M, Tellez N, Rodriguez MA, Yanes O, Lerin C, Diaz R, Plosch T, Tietge UJF, Jimenez-Chillaron JC. Epigenetic programming at the Mogat1 locus may link neonatal overnutrition with long-term hepatic steatosis and insulin resistance. FASEB J. 2018;32(11):6025–37.
38. Hui DY. Group 1B phospholipase A2 in metabolic and inflammatory disease modulation. Biochim Biophys Acta Mol Cell Biol Lipids. 2019;1864:784–8.
39. Erbilgin A, Siemers N, Kayne P, Yang WP, Berliner J, Lusis AJ. Gene expression analyses of mouse aortic endothelium in response to atherogenic stimuli. Arterioscler Thromb Vasc Biol. 2013;33:2509–17.
40. Zhang Y, Feng J, Yong J, Sun J. Zhang H [Experimental study on H2-Ab1 gene expression in the nasal mucosa of mice with allergic rhinitis]. Lin Chung Er Bi Yan Hou Tou Jing Wai Ke Za Zhi. 2014;28:327–31.
41. Sodek J, Ganss B, McKee MD. Osteopontin. Crit Rev Oral Biol Med. 2000;11:279–303.
42. Lim W, Jeong W, Kim J, Ka H, Bazer FW, Han JY, Song G. Differential expression of secreted phosphoprotein 1 in response to estradiol-17beta and in ovarian tumors in chickens. Biochem Biophys Res Commun. 2012;422:494–500.

Publisher's Note